Kaushlendra Dubey
Amit Gupta
Supreet Singh Bahga

Department of Mechanical Engineering, Indian Institute of Technology Delhi, Delhi, India

Received September 15, 2018
Revised December 3, 2018
Accepted December 14, 2018

Research Article

Scaling behavior in on-chip field-amplified sample stacking

Field amplified sample stacking (FASS) uses differential electrophoretic velocity of analyte ions in the high-conductivity background electrolyte zone and low conductivity sample zone for increasing the analyte concentration. The stacking rate of analyte ions in FASS is limited by molecular diffusion and convective dispersion due to nonuniform electroosmotic flow (EOF). We present a theoretical scaling analysis of stacking dynamics in FASS and its validation with a large set of on-chip sample stacking experiments and numerical simulations. Through scaling analysis, we have identified two stacking regimes that are relevant for on-chip FASS, depending upon whether the broadening of the stacked peak is dominated by axial diffusion or convective dispersion. We show that these two regimes are characterized by distinct length and time scales, based on which we obtain simplified nondimensional relations for the temporal growth of peak concentration and width in FASS. We first verify the theoretical scaling behavior in diffusion- and convection-dominated regimes using numerical simulations. Thereafter, we show that the experimental data of temporal growth of peak concentration and width at varying electric fields, conductivity gradients, and EOF exhibit the theoretically predicted scaling behavior. The scaling behavior described in this work provides insights into the effect of varying experimental parameters, such as electric field, conductivity gradient, electroosmotic mobility, and electrophoretic mobility of the analyte on the dynamics of on-chip FASS.

Keywords:
Dispersion / Field-amplified sample stacking / On-chip electrophoresis / Scaling analysis

DOI 10.1002/elps.201800392

Additional supporting information may be found online in the Supporting Information section at the end of the article.

1 Introduction

Miniaturization of capillary electrophoresis (CE) to planar microfluidic chips offers various advantages such as rapid analysis time, reduced sample volume, and increased selectivity [1–4]. A drawback of on-chip electrophoresis is that small depth of the microchannels, of order 10 μm, leads to a shorter path length for detection. This leads to reduced detection sensitivity in on-chip electrophoresis compared with conventional electrophoresis. Detection sensitivity can be significantly improved by coupling electrophoretic separation with on-line sample preconcentration methods [5], such as field-amplified sample stacking (FASS) [6–9], ITP [10–13], and pH gradient focusing [14]. Among various preconcentration methods, FASS is the most popular due to its simplicity and ease of implementation.

In FASS, a gradient in electrical conductivity of background electrolyte is established by creating adjacent zones of high- and low-concentration electrolyte, as shown in Fig. 1A. Sample analyte is initially mixed in the low-conductivity background electrolyte. Upon application of electric field, the analyte migrates across the conductivity gradient from low-conductivity zone to high-conductivity zone. The conductivity gradient establishes a gradient in the local electric field, which causes the analyte to migrate slowly in the high-conductivity zone (due to the lower local electric field) compared with that in the low-conductivity zone. This difference in electromigration velocity causes the analyte to stack in the high-conductivity zone. Typically in FASS, the concentration of analyte before and after stacking is significantly smaller than that of background electrolyte species and hence the analyte does not affect the conductivity

Correspondence: Supreet Singh Bahga, Department of Mechanical Engineering, Indian Institute of Technology Delhi, Delhi, 110016, India
Fax: +91 2658 2053
E-mail: bahga@mech.iitd.ac.in

Abbreviation: FASS, field amplified sample stacking

Color online: See the article online to view Figs. 2, 3, and 5 in color.

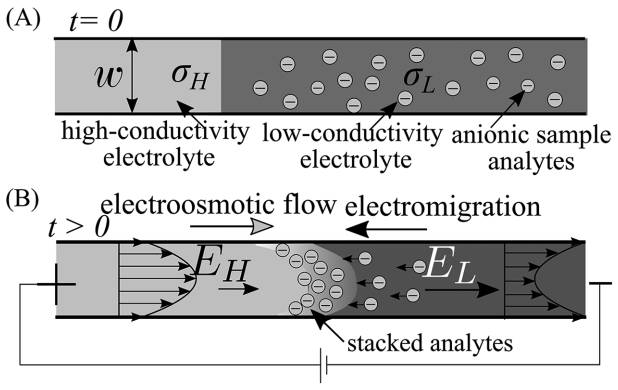

Figure 1. Schematic showing FASS in a single channel in the presence of EOF. (A) The initial condition at $t = 0$ with a sharp interface separating high- and low-conductivity zones. The anionic analyte is initially present in the low-conductivity zone. (B) Upon application of electric field, analyte ions stack near the interface separating high- and low-conductivity zones. The nonuniform EOF due to the conductivity gradient leads to dispersion of the stacked analyte. In addition, molecular diffusion also limits the rate of sample stacking.

gradient. Therefore, the ideal concentration enhancement is equal to the ratio of conductivities of high-conductivity electrolyte and low-conductivity sample ($\gamma > 1$), if the effects of pH and ionic strength [15] on electrophoretic mobility of analyte are neglected. FASS has been experimentally demonstrated to yield up to 1000-fold increase in detection sensitivity in on-chip electrophoresis [16].

In a theoretical scenario, if molecular diffusion and nonuniform fluid flow are absent, the sample analytes in FASS would attain their maximum permissible concentration instantaneously after they migrate into the high-conductivity zone. Thereafter, the leading front of stacked analyte zone migrates further into the high-conductivity zone, whereas the initial conductivity gradient remains stationary. In practice, an analyte in FASS takes a finite time to attain the maximum concentration. This is because the initial conductivity gradient and stacked sample zone broaden due to diffusion of background electrolyte species and analyte, respectively, which limit the rate at which the stacked analyte attains its maximum permissible concentration [17,18]. In addition, the mismatch of local EOF velocities in high- and low-conductivity regions lead to internal pressure gradients that drive nonuniform secondary fluid flow. The resulting nonuniform fluid flow causes convective dispersion of the stacked analyte and further reduces the stacking efficiency. The effect of convection–electromigration–diffusion phenomenon on stacking performance in FASS was first modeled by Burgi and Chien [19]. They presented an algebraic model for the variance of the stacked peak by accounting for sample accumulation, axial diffusion, and Taylor dispersion [20] due to nonuniform EOF and validated the theoretical predictions with experimental observations. Subsequently, Bharadwaj and Santiago [21] presented an unsteady model, based on Taylor dispersion analysis, to predict the spatiotemporal evolution of cross-sectional area-averaged species concentrations in FASS. Bharadwaj and Santiago also compared their model predictions with time-resolved experiments of on-chip FASS.

The mathematical models of Burgi and Chien [19] and Bharadwaj and Santiago [21] provide key insights into the transient growth of concentration and peak width of the stacked analyte. Because these models are based on Taylor dispersion analysis, they are strictly applicable for times that are significantly larger than the time scale associated with transverse (or radial) diffusion and peak widths that are significantly larger than the transverse dimensions of the channel. As shown by Ajdari et al. [22], in microfluidic channels, which often have a larger width compared with the depth, the hydrodynamic dispersion is controlled by the larger of the transverse dimensions. That is, for a shallow microchannel with a width w and depth $d/w \ll 1$, the Taylor dispersion regime is attained when the peak width $\ell \gg w$ and for times $t \gg w^2/D$, where D is the molecular diffusivity of the solute [23]. In practical on-chip electrophoresis experiments, where analysis times are short, and preconcentration using FASS is done only for a short time before electrophoretic separation, these assumptions for Taylor dispersion analysis often do not hold. Therefore, the long-time Taylor dispersion limit may not be attained in on-chip FASS within the timeframe of analysis if EOF is present; the long-time limit is usually attained in conventional electrophoresis, where stacking times and peak widths are large. This is evidenced by the experimental images of on-chip FASS in the presence of EOF, presented by Yang and Chien [24] and Bharadwaj and Santiago [21], which clearly show the strong convective dispersion of stacked analyte. In these experiments, the stacked analyte did not have sufficient time to diffuse in the transverse direction to diminish the concentration gradients established by nonuniform EOF, suggesting that the Taylor dispersion regime was not attained. We note that Bharadwaj and Santiago [21] presented another set of experiments wherein EOF was significantly suppressed to prevent convective dispersion and validate their mathematical model. Given that the previously described theoretical description of FASS in the long-time Taylor dispersion limit is not observed in on-chip experiments, there is still a lack of theoretical understanding of the dynamics of on-chip FASS. In particular, the relevant time scales and the scaling behavior of peak concentration and width with experimental parameters such as electric field, conductivity gradient, and EOF mobility have not been described previously.

In the current work, we elucidate the scaling behavior in FASS based on theoretical scaling analysis, numerical simulations, and time-resolved on-chip sample stacking experiments. We identify two distinct sample stacking regimes depending upon whether the axial diffusion or convective dispersion dominates peak broadening. We begin by presenting the relevant length and time scales in FASS. We then use these characteristic length and time scales to express the dependence of peak concentration and width in nondimensional form. Next, we verify the theoretical

scaling analysis with multidimensional numerical simulations of on-chip FASS in the presence of EOF. We then present experimental data of transient growth in peak concentration and peak width in FASS for varying electric fields, conductivity gradients, and EOF mobility. We show that if simulation and experimental data of temporal growth of peak concentration and width for varying experimental conditions are plotted using dimensionless variables identified from scaling analysis, all data collapse on respective curves for the two stacking regimes.

2 Theory

2.1 Problem description

We consider FASS of a single anionic analyte in a wet-etched, glass microchannel with a D-shaped cross-section. The width and centerline depth of the microchannel are w and d, respectively, and we assume that the microchannel is shallow ($d \ll w$). Initially, a sharp discontinuous boundary is established between high-conductivity electrolyte zone and low-conductivity sample zone, as shown schematically in Fig. 1A. The high- and low-conductivity electrolytes consist of an anionic and a cationic background electrolyte species. That is, the background electrolyte is a binary electrolyte. The initial concentration of the anionic analyte c_0, mixed with the low-conductivity electrolyte, is taken to be significantly smaller than the concentrations of background electrolyte species so that migration of analyte does not affect the local conductivity. At $t = 0$, electric field is applied pointing from the high-conductivity electrolyte toward the low-conductivity sample zone. This causes the negatively charged analyte ions to stack near the interface between high- and low-conductivity zones. The external electric field also drives an EOF in the direction opposite to the motion of analyte ions, as shown in Fig. 1B. The gradient in electrical conductivity leads to a gradient in the local electric field and electroosmotic slip velocity. This mismatch in EOF leads to an internal pressure gradients that drive nonuniform pressure-driven flow. The resulting velocity profiles in high- and low-conductivity zones are illustrated in Fig. 1B. If the magnitude of EOF velocity is higher than the electromigration velocity of the analyte, as is the case in our experiments, the stacked analyte convects downstream along the direction of EOF. The interface separating high- and low-conductivity regions also convects along with the EOF. Note that a gradient in binary electrolyte does not electromigrate unless surface conduction is dominant [25, 26]. In the FASS, differential electromigration speed of analyte in high- and low-conductivity zones is responsible for the stacking. On the other hand, molecular diffusion and convective dispersion of analyte and conductivity field act in a way to disperse the stacked zone and reduce the preconcentration level. As illustrated in Fig. 1, here we consider a semiinfinite sample zone for which the analyte continues to stack over time and peak width increases continuously with time. At a later time, the stacked zone attains its maximum concentration and thereafter the only effect of stacking is the increase in width of stacked analyte zone. Here, we are interested in understanding the temporal growth of peak concentration and peak width as functions of various experimental parameters, such as electric field, conductivity gradient, channel dimensions, electroosmotic mobility, and electrophoretic mobility of the analyte.

2.2 Length and time scales in FASS

One way to theoretically describe the dynamics of the FASS process is by using 3D convection–electromigration–diffusion equations along with appropriate initial and boundary conditions [27]. Besides these conservation laws, equations for acid–base equilibrium and ionic strength corrections are required to model the effect of pH and ionic strength of effective mobility and diffusivity of ionic species [15]. To keep our focus on the essential physics of FASS without going into finer details of electrolyte chemistry, in our theoretical analysis we consider mobility and diffusivity of ionic species to be constant. This is a reasonable assumption when the species are fully ionized or the electrolytes are well buffered. Moreover, rather than solving the complicated partial differential equations that govern the transport phenomena in FASS, we approach the problem only using dimensional analysis.

First, we look at the relevant length and time scales in the FASS process, as described in Section 2.1 and illustrated in Fig. 1. In the current problem, channel width w and depth d are the two obvious length scales. Because we have assumed depth to be significantly smaller than the width, any variation in species concentrations along the depth will quickly diminish due to rapid molecular diffusion over a short time scale of d^2/D, where D denotes the diffusivity of analyte. Therefore, depth d does not affect the dynamics of sample stacking and hereafter we do not consider the depth in our dimensional analysis. In the current problem, there is no external length scale in the axial direction because the initial interface separating semiinfinite zones of high and low conductivity is sharp. However, there is an intrinsic axial length scale δ associated with the sample stacking phenomena, which arises due to the balance between electromigration and diffusive fluxes,

$$\mu \frac{\partial}{\partial x}(c\,E) \sim D\frac{\partial^2 c}{\partial x^2}, \tag{1}$$

where c denotes the analyte concentration, E is the electric field, x is the axial coordinate, and μ and D denote the electrophoretic mobility and diffusivity of the analyte, respectively. Because the analyte migrates in the high-conductivity zone, the relevant scale for electric field in Eq. (1) is the local electric field in the high-conductivity zone, denoted by E_{H}. If the length of the low-conductivity sample zone is significantly large compared with the length of the high-conductivity zone, then the electric field in the sample zone E_{L} is almost equal to the average electric field applied in the channel, that is, $E_{\mathrm{s}} \approx E$. In

such cases, the electric field in the high-conductivity zone can be approximated as $E_H \approx E/\gamma$ because continuity of current dictates that $\sigma_H E_H = \sigma_L E_L$. Here, σ_H and σ_L are the conductivities of high- and low-conductivity zones and $\gamma = \sigma_H/\sigma_L$. Next, using Eq. (1) we can obtain the intrinsic length scale δ as,

$$\frac{\mu E}{\delta\gamma} \sim \frac{D}{\delta^2}, \quad \delta \equiv \frac{\gamma D}{\mu E}. \tag{2}$$

Note that the diffusivity is related with the electrophoretic mobility by the Nernst–Einstein relation $D = \mu kT/(ze)$, where z is the valance number and $kT/e = 25.7$mV is the thermal voltage at temperature $T = 298$ K.Therefore, the length scale δ can alternatively be interpreted as the ratio of thermal voltage to the local electric field in the high-conductivity zone.

The intrinsic time scale τ_s for sample stacking can be defined using the length scale δ as,

$$\tau_s \equiv \frac{\delta^2}{D} = \frac{\gamma^2 D}{\mu^2 E^2}. \tag{3}$$

This time scale can be interpreted as the time scale for the analyte to diffuse over length δ. Due to the balance of electromigration and diffusive fluxes, τ_s also corresponds to the time taken for electromigration across the length δ. The time scale for diffusion of the analyte over the channel width is $\tau_d = w^2/D$, and the time to move the distance w by electromigration is $\tau_{em} = w\gamma/(\mu E)$. Besides τ_d, we have another diffusion time scale $\tau_{bg} = w^2/D_\sigma$, corresponding to the diffusion of the conductivity field. For a binary electrolyte, the effective diffusivity is given by $D_\sigma = D_+ D_-(z_+ - z_-)/(z_+ D_+ - z_- D_-)$, where $z_\pm$and $D_\pm$ denote the valence and diffusivity of anions and cations of background electrolyte, respectively. Typically, the diffusivities of analytes and background electrolyte species are of the same order of magnitude and so it the case of τ_d and τ_{bg}. To obtain the timescale corresponding to nonuniform EOF, we note that the mean EOF velocity in the channel is $\mu_{eof} E$, where μ_{eof} is the electroosmotic mobility of the channel surface and E is the average electric field. The mismatch in local and mean EOF is highest in the high conductivity zone ($\mu_{eof} E(\gamma - 1)/\gamma$) and this drives a strong pressure-driven flow in the high-conductivity zone, which causes sample dispersion. Therefore, the characteristic time scale for convective dispersion due to nonuniform EOF can be taken as $\tau_{eof} = w\gamma/(\mu_{eof} E(\gamma - 1))$. We note that the coupling of electric field and conductivity gradients can lead to electroviscous flow, which has an associated electroviscous time scale [28, 29]. Here, we neglect the electroviscous time scale because the dispersion of analyte peak due to electroviscous flow is usually negligible compared with that due to nonuniform EOF [21]. Based on the various length and time scales, we now describe the dynamics of FASS in two limits: (i) when axial diffusion dominates convective dispersion and (ii) when convective dispersion dominates axial diffusion.

2.3 Diffusion-dominated regime

The relative importance of diffusion and convection can be described using the Peclet number Pe, which is defined as the ratio of diffusion and convection time scales, $Pe \equiv \tau_d/\tau_{eof} = (\gamma - 1)\mu_{eof} E w/(\gamma D)$. From the Taylor dispersion analysis, it is known that convective dispersion appears only above Peclet numbers of order 10 [30]. Therefore, at low Peclet numbers, the effect of EOF on peak concentration and width can be ignored. In this diffusion-dominated regime, the only effect of EOF is to convect the stacked analyte zone downstream. That is, when convective dispersion can be neglected the stacking process can be considered to be essentially 1D along the channel axis. Therefore, the dynamics of FASS depends only on the intrinsic length scale δ (defined by Eq. (2)) and not on the channel width w. Similarly, the time scales that depend on w are not relevant in the diffusion-dominated regime and the only relevant time scale is τ_s, as defined in Eq. (3). Denoting the peak concentration by c_{max} and the FWHM as ℓ, we can write

$$\frac{c_{max}}{c_0} = f\left(\frac{t}{\tau_s}, \gamma, \frac{D_\sigma}{D}\right), \quad \frac{\ell}{\delta} = g\left(\frac{t}{\tau_s}, \gamma, \frac{D_\sigma}{D}\right), \tag{4}$$

where t is the time and c_0 is the initial analyte concentration. In these dimensionless relations, the parameter D_σ/D is fixed by choice of electrolyte chemistry and the sample analyte. In practice, the desired concentration enhancement is obtained by varying the conductivity ratio γ and electric field. The effect of electric field on peak concentration and width is accounted for by τ_s and δ.

The exact functional dependence of dimensionless peak concentration and width can be determined only from numerical simulations or experiments. However, we can make further simplifications to Eq. (4) by noting that for a given D_σ/D, the temporal growth rate of peak concentration and width is primarily governed by the time scale τ_s, which already accounts for the conductivity ratio γ. The only other effect of conductivity ratio γ is to increase the preconcentration level when nonuniform EOF is negligible. Therefore, we can simplify Eq. (4) for a fixed value of D_σ/D as

$$\frac{c_{max}/c_0 - 1}{\gamma - 1} = f(t/\tau_s), \quad \frac{\ell}{\delta} = g\,(t/\tau_s)\,. \tag{5}$$

In practice, due to limited channel length available for preconcentration on a microfluidic device, it is important to consider the peak concentration and width as a function of the axial location of the stacked peak x. The stacked peak primarily migrates due to EOF $x \approx \mu_{eof} Et$, that is, $t/\tau_s = x\mu^2 E/(\mu_{eof}\gamma^2 D)$. Here, we have neglected the migration of peak maxima due to electromigration as the electrophoretic velocity of the analyte in high-conductivity zone ($\mu E/\gamma$) is small. Therefore, Eq. (5) can be written in terms of peak location x as

$$\frac{c_{max}/c_0 - 1}{\gamma - 1} = f\left(\frac{\mu^2 E}{\mu_{eof}\gamma^2 D}x\right), \quad \ell = \frac{\gamma D}{\mu E} g\left(\frac{\mu^2 E}{\mu_{eof}\gamma^2 D}x\right) \tag{6}$$

As f is a monotonically increasing function, this equation shows that at a given axial peak location x the

preconcentration efficiency is higher at the higher electric field. On the other hand, the peak width ℓ at a given location x shows a weak dependence on the electric field, as Eq. (6) shows that higher value of the function g at high E is negated by the factor $1/E$. Therefore, increasing the electric field in diffusion-dominated regime yields higher preconcentration at a fixed channel location without any significant change in the peak width.

2.4 Convection-dominated regime

At high electric fields, nonuniform EOF leads to severe convective dispersion of the stacked peak. This regime corresponds to large Peclet number $(\gamma - 1)\mu_{eof} E w/(\gamma D) \gg 1$. At short times($t \ll w^2/D$), convective dispersion establishes strong transverse concentration gradients. Subsequently, over times scales of order, $\tau_d = w^2/D$, the transverse concentration gradients diminish due to molecular diffusion along the channel width. In on-chip FASS, typically the preconcentration time is so short that the long-time Taylor dispersion regime ($t \gg w^2/D$) is never established. Therefore, here we focus only on the short time limit characterized by strong transverse concentration gradients. While the concentration of stacked analyte varies significantly in the transverse direction, we are interested in the area-averaged concentration. This is because the detection methods in electrophoresis such as fluorescence, UV, and conductivity detection give signals that depend on the average concentrations within the detection region [23].

In the convection-dominated regime, the relevant length scale is the channel width w because of strong transverse concentration gradients. The important time scale in this regime is $\tau_{eof} = w\gamma/(\mu_{eof} E(\gamma - 1))$ corresponding to nonuniform EOF, which is responsible for the dispersion of stacked analyte peak. From the dimensional analysis, we can write that

$$\frac{c_{max}}{c_0} = f\left(\frac{t}{\tau_{eof}}, \frac{\tau_d}{\tau_{eof}}, \frac{\tau_d}{\tau_{bg}}, \frac{\tau_{eof}}{\tau_{em}}, \gamma\right) = f\left(\frac{t}{\tau_{eof}}, Pe, \frac{D_\sigma}{D}, \frac{\mu}{\mu_{eof}}, \gamma\right), \tag{7}$$

where c_{max} is the maximum area-averaged concentration of the stacked peak. Similarly, the FWHM of area-averaged concentration ℓ can be described in dimensionless form as

$$\frac{\ell}{w} = g\left(\frac{t}{\tau_{eof}}, Pe, \frac{D_\sigma}{D}, \frac{\mu}{\mu_{eof}}, \gamma\right). \tag{8}$$

Again, in these equations D_σ/D is governed by the choice of background electrolyte and the analyte. Similarly, the ratio of electrophoretic mobility to electroosmotic mobility μ/μ_{eof} cannot be varied during the experiment as it depends on the choice of background electrolyte and microchannel substrate. In addition, we may neglect the dependence of Peclet number Pe in Eqs. (7) and (8). This is because, as pointed out by Barenblatt [31], in dimensional analysis if a certain dimensionless parameter is significantly large or small compared with unity, it may be assumed to be nonessential. In our case, $Pe \gg 1$ and its absolute value may not affect the dynamics of FASS in the short-time regime. Lastly, we can also exclude additional dependence of dimensionless concentration and peak width on the conductivity ratio γ, because its effect is already accounted for in the time scale for EOF τ_{eof}. This assumption can also be justified by noting that in FASS, the analyte stacked per unit cross-sectional area is $\mu E_L c_0 t \approx \mu E c_0 t$. Because the stacking of analyte causes the peak concentration and peak width to grow, $c_{max}\ell \sim \mu E c_0 t$. In the convection-dominated regime at short times, the peak width ℓ is governed by convective dispersion due to nonuniform EOF and hence the peak concentration also depends on the time scale of nonuniform EOF. Other than generating the nonuniform EOF, there is no additional dependence of peak concentration and width on the conductivity ratio γ. Therefore, for fixed values of D_σ/D and μ/μ_{eof}, we can simplify Eqs. (7) and (8) to

$$\frac{c_{max}}{c_0} = f(t/\tau_{eof}), \quad \frac{\ell}{w} = g(t/\tau_{eof}). \tag{9}$$

For practical conductivity ratios used in FASS, $\gamma \sim \mathcal{O}(10)$, the time scale for nonuniform EOF $\tau_{eof} = w\gamma/(\mu_{eof} E(\gamma - 1))$ can be approximated as $\tau_{eof} \approx w/(\mu_{eof} E)$. Therefore, $t/\tau_{eof} \approx x/w$, where x is the axial location of the stacked analyte peak. Interestingly, this suggests that in the presence of strong EOF, the peak concentration and width at a fixed location in the microchannel are independent of the conductivity ratio. For the same reason, to obtain high preconcentration in on-chip FASS, it is necessary to suppress the EOF so that stacking takes place in the low Peclet number regime described in Section 2.3.

2.5 Numerical simulations

To confirm the scaling behavior in diffusion- and convection-dominated regimes, we performed 2D simulations of FASS using the COMSOL Multiphysics software (COMSOL AB, Stockholm, Sweden). We performed simulations of FASS in a cross-shaped microfluidic channel having same channel lengths and widths as those of the microchannel used in our experiments (Fig. 3). Initially, at $t = 0$ s, a sharp conductivity gradient was generated between high- and low-conductivity electrolytes, with a conductivity ratio $\gamma = 4.5$. An anionic analyte, with $\mu = -30 \times 10^{-9}$ m^2/V/s, was initially mixed in the low-conductivity zone at a concentration of 1 μM. Initially, the mixture of analyte and low-conductivity electrolyte filled the main channel. When external electric field pointing from high- to low-conductivity zone is applied, the anionic analyte stacks at the conductivity gradient, while EOF causes high-conductivity electrolyte to displace the low-conductivity electrolyte. A detailed description of the governing equations, boundary and initial conditions, and simulation methodology has been provided in the Supporting Information.

We performed 2D simulations on-chip FASS for varying Peclet numbers ranging from P_e=1 to 20. Figure 2A and its inset show the variation of dimensionless peak

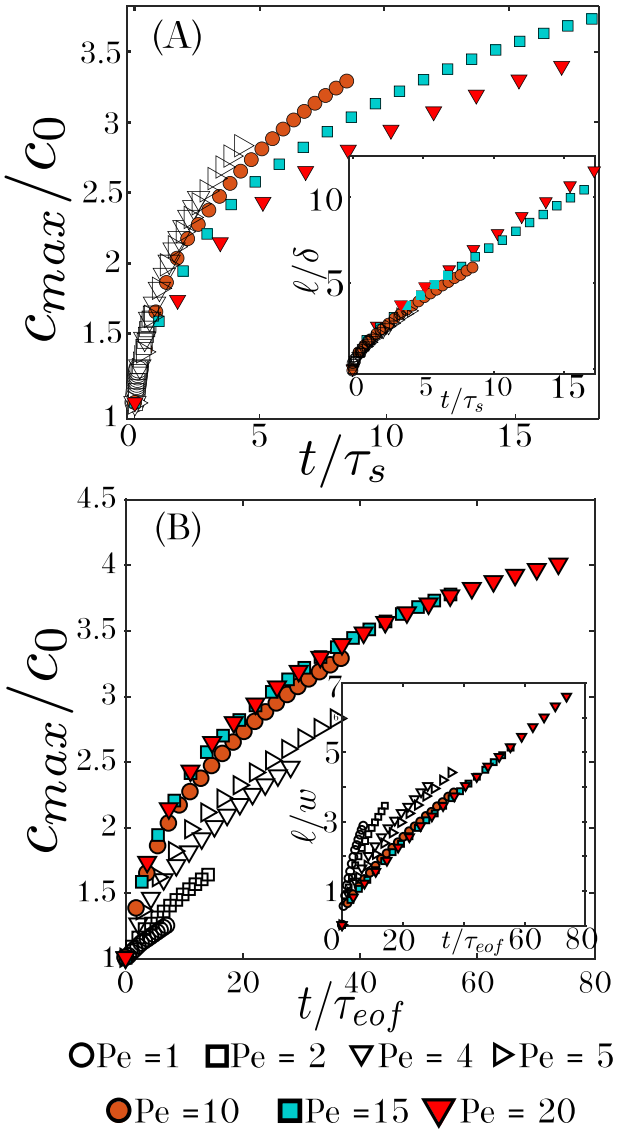

Figure 2. Temporal evolution of peak concenentration c_{max} and peak width ℓ obtained from 2D simulations for varying Peclet number, $Pe = 1$–20. (A) The dimensionless peak concentrations at low Peclet numbers ($Pe = 1$, 2, 4, and 5) collapse on a single curve when plotted versus dimensionless time t/τ_s, that is, for diffusion-dominated regime. Inset of (A) shows that FWHM at low Peclet numbers also agrees with the theoretical scaling given by Eq. (5) for diffusion-dominated regime. (B) The dimensionless peak concentrations at higher Peclet numbers ($Pe = 15$ and 20) collapse on a single curve when plotted against dimensionless time t/τ_{eof} corresponding to convection-dominated regime. Inset of (B) shows that FWHM at higher Peclet numbers also agrees with the theoretical scaling for convection-dominated regime, given by Eq. (9).

concentration c_{max}/c_0 and FWHM ℓ/δ versus dimensionless time t/τ_s, based on the scaling for diffusion-dominated regime. On the other hand, Fig. 2B and its inset show the variation of dimensionless peak concentration c_{max}/c_0 and FWHM ℓ/w versus dimensionless time t/τ_{eof}, based on the scaling for convection-dominated regime. As shown in Fig. 2A, at low Peclet numbers ($Pe = 1$, 2, 4, and 5), simulation data for peak concentration and FWHM collapse on a single curve when plotted using the dimensionless quantities corresponding to the diffusion-dominated regime, confirming the scaling behavior described in Eq. (5). Similarly for high Peclet numbers ($Pe = 15$ and 20), the simulation data collapse when plotted using the dimensionless quantities corresponding to the convection-dominated regime (Fig. 2B), confirming the theoretical scaling given by Eq. (9). The data for $Pe = 10$ appears to agree with scaling behavior for both diffusion- and convection-dominated regimes, albeit with some deviations. This suggests that for $Pe = 10$, both diffusive and convective effects are relevant and hence it marks the transition between diffusion- and convection-dominated regimes. Besides these 2D simulations, in the Supporting Information, we also provide 1D simulations of FASS using SPRESSO (Stanford Public Release Electophoretic Separation Solver) simulation tool [32–34] for the case when EOF is absent. These 1D simulations also confirm the scaling behavior predicted by Eq. (5) for diffusion-dominated regime. In particular, these 1D simulations clearly show that, in the diffusion-dominated regime, the preconcentration efficiency and FWHM do not depend on the conductivity gradient, as given by Eq. (5).

3 Experiments

We performed a series of on-chip FASS experiments to validate the scaling behavior for the convection-dominated regime, as described in Section 2.4. To validate the scaling for diffusion-dominated regime, as described in Section 2.3, we have used published experimental data of Bharadwaj and Santiago [21], who performed similar on-chip FASS experiments but with suppressed EOF.

3.1 Materials and methods

Experiments were conducted in a standard cross-shaped, glass microchannel (Micronit, The Netherlands), as shown schematically in Fig. 3A. The microchannels connecting the north (N), south (S), and west (W) reservoirs to the junction were 5 mm long, and the main channel connecting the junction to the east E reservoir was 35 mm long. All the channels were isotropically etched with a D-shaped cross-section of 50 μm width and 20 μm depth. The experiments were performed in two steps: (i) injection to establish a conductivity gradient and (ii) FASS for sample preconcentration. Figure 3A shows the first step in which the E reservoir was filled with the low-conductivity sample electrolyte consisting of background electrolyte species and the analyte. The N and W reservoirs were filled with the high-conductivity electrolyte. Thereafter, vacuum was applied at the south reservoir to generate a sharp conductivity gradient at the junction, as shown schematically in Fig. 3A. Once the initial conductivity gradient was established, an axial electric field was applied between W and E reservoirs by applying potential difference

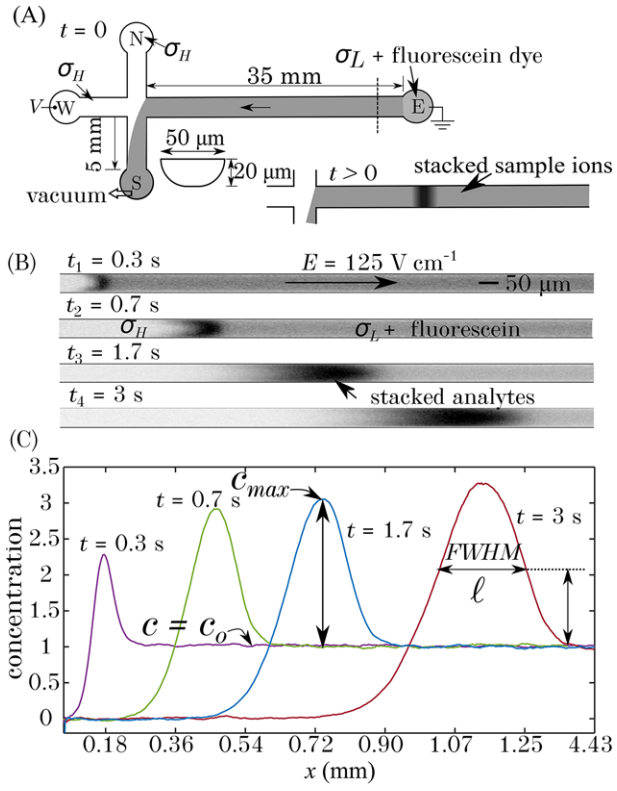

Figure 3. (A) Schematic showing the injection protocol for on-chip FASS experiment in a cross-shaped microchannel. (B) Representative CCD images for $\gamma = 4.5$ at various times showing sample stacking and dispersion due to nonuniform EOF. (C) Area-averaged analyte concentration with time. Here, c_{max} represents the maximum concentration, and FWHM (ℓ) represents the peak width at half of the stacked peak above the initial concentration, $c = c_0$.

on the platinum electrodes dipped in these reservoirs, using a high voltage power supply (Ionics, India; maximum 5 kV and 10 mA). Upon application of electric field, the vacuum is released, and this leads to stacking of the analyte in the channel connecting the junction and E reservoir. We note that due to the very high hydraulic resistance of the main channel, small mismatch in liquid's level in the reservoirs do not lead to any significant pressure-driven flow in the main channel.

For all our experiments, the high-conductivity electrolyte consisted of 30 mM sodium hydroxide and 100 mM MOPS (measured conductivity $\sigma_H = 0.193$ S/m and pH 6.8). For one set of experiments corresponding to $\gamma = 4.5$, the low-conductivity electrolyte consisted of 6 mM sodium hydroxide and 30 mM MOPS (measured conductivity $\sigma_L = 4.3 \times 10^{-2}$ S/m and pH 6.6). Another set of experiments were performed with $\gamma = 8.8$, for which the low-conductivity electrolyte consisted of 3 mM sodium hydroxide and 10 mM MOPS (measured conductivity $\sigma_L = 2.2 \times 10^{-2}$ S/m and pH 6.8). The high- and low-conductivity electrolyte solutions were prepared by diluting 1 M stock solution each of MOPS (Sigma Aldrich, USA) and sodium hydroxide (CDH, India) solution using Millipore deionized water. The analyte was 30 μM fluorescein anion of sodium fluorescein salt (CDH, India).

We observed the stacking process using an inverted epifluorescence microscope (Nikon Eclipse Ti-U, Japan) equipped with a mercury arc lamp, 4× objective (Plan Fluor, WD = 17.2 mm, NA = 0.13), and Nikon B2-A filter set (420–495 nm band pass excitation filter and 510 nm longpass barrier filter). The time resolved images were captured using a 14-bit, 1092 × 1040 pixel array CCD camera (PCO pixelfly; PCO AG, Germany) with an exposure time of 10 ms and frame rate of 27 fps. Prior to data analysis, we corrected all the CCD images of the stacked fluorophore for systematic errors by subtracting a dark-field image and normalizing the resulting data with a flat-field image. We also performed a series of experiments to calibrate the fluorescence intensity with respect to the fluorescein concentration. These calibration experiments showed that the fluorescence intensity is directly proportional to the sample concentration for the range of fluorescein concentrations expected during our FASS experiments. The maximum concentration and FWHM of the peak were calculated after averaging the instantaneous snapshots over the channel width, as shown in Fig. 3B and C.

4 Results and discussion

4.1 Diffusion-dominated regime

First, we validate the scaling behavior described by Eq. (5) for low Peclet numbers with time-resolved, on-chip FASS experiments of Bharadwaj and Santiago [21]. The experimental method of Bharadwaj and Santiago was similar to ours, described in Section 4, except that EOF in their experiments was suppressed significantly by treating the wet-etched glass microchannel (width 50 μm and depth 20 μm) with poly(ethylene oxide). In these experiments, the background electrolyte was sodium HEPES and the analyte was bodipy dye ($\mu = -19 \times 10^{-9} m^2/V/s$). Here, we analyze the experimental data for conductivity ratio $\gamma = 9$, for varying electric fields $E \approx E_L$ =188, 294, and 588 V/cm. Due to EOF suppression, the measured EOF mobility in these experiments was 0.3×10^{-9} $m^2/V/s$, which is two orders of magnitude smaller than that of the untreated glass surface. Therefore, the maximum Peclet number in these set of experiments corresponding to the electric field of 588 V/cm was 1.6, which is an order of magnitude smaller than the Peclet number required for appreciable convective dispersion.

Figure 4 shows the experimentally measured dimensionless peak concentration c_{max}/c_0 versus dimensional time t for varying electric field values. The growth of peak concentration with time is faster at higher electric fields. When the same experimental data of dimensionless peak concentration c_{max}/c_0 is plotted versus dimensionless time t/τ_s, as shown in the inset of Fig. 4, the data collapse on a single curve. This validates the scaling behavior described by Eq. (5). That is, the stacking dynamics in FASS experiments with suppressed EOF are governed by the stacking time scale τ_s. We note that

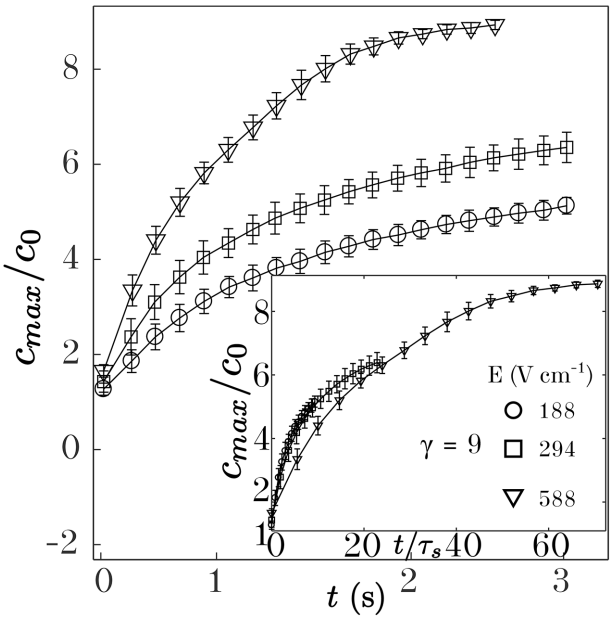

Figure 4. Variation of peak concentration versus time in on-chip FASS experiments of Bhardwaj and Santiago [21]. These experiments were performed for $\gamma = 9$ and by suppressing EOF. The inset shows that all data collapse on a single curve when plotted using dimensionless variables (c_{max}/c_0 versus t/τ_s) .

slight deviation of experimental data at E =588 V/cm from the experiments at lower values of electric field might be due to the dispersive effects of Joule heating and 3D nature of flow near the channel junction, which become important at higher electric fields.

4.2 Convection-dominated regime

Next, we validate the scaling behavior described by Eq. (9) for high Peclet number regime, where convective dispersion dominates. In these experiments, EOF was not suppressed and this resulted in the significant dispersion of analyte peak due to nonuniform EOF, as shown in Fig. 3B. We estimated the EOF mobility using the migration speed of the analyte peak, as the peak migrates primarily due to strong EOF. The EOF mobility in these set of experiments was 57×10^{-9} m^2/V/s. Figure 5 shows experimentally measured peak concentrations and peak widths for conductivity ratios $\gamma = 4.5$ and 8.8 and electric field values of $E = 50$, 75, and 125 V/cm. Therefore, the minimum Peclet number for these experiments, corresponding to the electric field of 50 V/cm and $\gamma = 4.5$, was 12 (taking diffusivity of fluorescein $D = 9 \times 10^{-10}$ m^2/s [35]). In Fig. 5, three realizations of each experiment are shown, and the data show good repeatability of experiments. As shown in the inset of Fig. 5A, the sample stacking is faster at higher electric fields for both conductivity ratios. When the same data for the temporal evolution of peak concentration is plotted using dimensionless variables, that

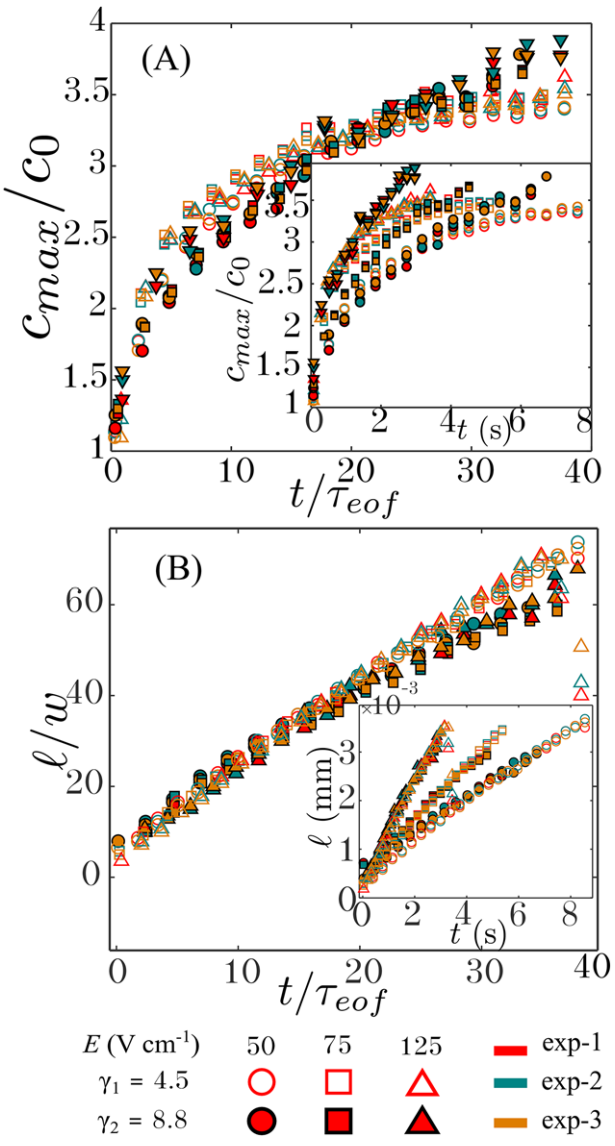

Figure 5. Experimental validation of scaling behavior for peak concentration c_{max} and FWHM ℓ in the convection-dominated regime. Insets of (A) and (B) show the effect of the electric field and the conductivity ratio γ on the measured peak concentration and FWHM, respectively. The growth of peak concentration and width is faster at higher electric field, but it does not show significant dependence on conductivity ratio. (A and B) The data for varying electric field and conductivity ratios collapse on single curve when plotted using dimensionless variables given in Eq. (9).

is, c_{max}/c_0 versus t/τ_{eof}, the experimental data collapse on to a single curve. Moreover, the variation of c_{max}/c_0 versus t/τ_{eof} for $\gamma = 4.5$ and 8.8 for varying electric fields ($Pe = 12$, 18, and 30 for $\gamma = 4.5$and $Pe = 14$, 21, and 35 for$\gamma = 8.8$) is almost identical. Similarly, when the data for FWHM versus time (shown in Fig. 5B) are plotted using dimensionless variables, that is, ℓ/w versus t/τ_{eof}, all experimental data at varying electric field and conductivity ratio fall on a single curve.

This validates the theoretical scaling behavior described by Eq. (9) when the convective dispersion is dominant. That is, the stacking dynamics of FASS in the presence of strong EOF and for short times is governed solely by the time scale for nonuniform EOF τ_{eof}.

5 Concluding remarks

We have presented a scaling analysis of the dynamics of on-chip FASS and validated it with a large set of time-resolved experiments of sample stacking for varying electric field values, conductivity gradients, and EOF mobility. First, we described the ideal dynamics of FASS, which is observed when EOF is suppressed, and axial diffusion dominates broadening of the stacked peak. In this low Peclet number regime, the intrinsic time scale $\tau_s = \gamma^2 D/(\mu^2 E^2)$ governs the transient growth of peak concentration and width. Based on this scaling argument, we showed that an increase in the electric field in diffusion-dominated regime yields maximum concentration enhancement γ in a shorter time and smaller distance traveled by the stacked peak.

When EOF is not suppressed, the mismatch in local electroosmotic slip velocity in high- and low-conductivity zones leads to a nonuniform flow that causes unwanted convective dispersion of the stacked analyte. In on-chip FASS, where preconcentration time is often short, slow molecular diffusion is unable to diminish transverse concentration gradients generated by the nonuniform flow. Therefore, unlike in conventional capillary electrophoresis where analysis time is large, the Taylor dispersion regime is not attained in on-chip FASS. We have shown that in this high Peclet number, convection-dominated regime, the dynamics of stacking is governed solely by the time scale for nonuniform EOF, $\tau_{eof} = w\gamma/(\mu_{eof} E(\gamma - 1))$. As a consequence of this scaling behavior, even though higher electric fields lead to faster stacking, the peak concentration for a fixed axial location of the stacked peak is independent of electric field. Moreover, increasing the conductivity ratio does not improve the stacking at a fixed peak location.

We have presented a detailed validation of scaling behavior in diffusion- and convection-dominated regimes using time-resolved data of peak concentration and width from numerical simulations and experiments of on-chip FASS. The scaling behavior described in this work suggests that to achieve large concentration enhancement in on-chip FASS, the convection-dominated regime must be avoided. That is, experimental conditions should be chosen either to ensure low Peclet number or by increasing the channel length and analysis time to ensure that the Taylor dispersion regime is achieved. However, we note that in many practical applications, such as large volume sample stacking [36], EOF is used as a means to couple FASS with electrophoretic separation. In such cases, convective dispersion of the stacked analyte is unavoidable. Therefore, the scaling behavior described here for both low and high Peclet number regimes is of practical significance.

The authors wish to thank the Science and Engineering Research Board (SERB), Government of India for providing the financial support through the project grant SB/FTP/ETA-308/2013.

The authors have declared no conflict of interest.

6 References

[1] Lichtenberg, J., Verpoorte, E., Rooij, N. F. D., *Electrophoresis* 2001, *22*, 258–271.

[2] Hardt, S., Schönfeld, F., *Microfluidic Technologies for Miniaturized Analysis Systems*, Springer Science & Business Media, Berlin, Germany, 2007.

[3] Dolnik, V., Liu, S., Jovanovich, S., *Electrophoresis* 2000, *21*, 41–54.

[4] Bharadwaj, R., Santiago, J. G., Mohammadi, B., *Electrophoresis* 2002, *23*, 2729–2744.

[5] Osbourn, D. M., Weiss, D. J., Lunte, C. E., *Electrophoresis* 2000, *21*, 2768–2779.

[6] Zhang, C. X., Thormann, W., *Anal. Chem.* 1996, *68*, 2523–2532.

[7] Chien, R. L., Burgi, D. S., *J. Chromatogr.* 1991, *559*, 141–152.

[8] Chien, R. L., Burgi, D. S. *Anal. Chem.* 1992, *64*, 489A–496A.

[9] Gong, M., Wehmeyer, K. R., Limbach, P. A., Arias, F., Heineman, W. R., *Anal. Chem.* 2006, *78*, 3730–3737.

[10] Bhattacharyya, S., Gopmandal, P. P., Baier, T., Hardt, S., *Phys. Fluids* 2013, *25*, 022001.

[11] Gopmandal, P. P., Bhattacharya, S., *J. Fluids Eng.* 2015, *137*, 081202.

[12] Bahga, S. S., Santiago, J. G., *Analyst* 2013, *138*, 735–754.

[13] Shintaku, H., Nishikii, H., Marshall, L. A., Kotera, H., Santiago, J. G., *Anal. Chem.* 2014, *86*, 1953–1957.

[14] Britz-McKibbin, P., Chen, D. D., *Anal. Chem.* 2000, *72*, 1242–1252.

[15] Bahga, S. S., Bercovici, M., Santiago, J. G., *Electrophoresis* 2010, *31*, 910–919.

[16] Jung, B., Bharadwaj, R., Santiago, J. G., *Electrophoresis* 2003, *24*, 3476–3483.

[17] Chien, R. L., Helmer, J. C., *Anal. Chem.* 1991, *63*, 1354–1361.

[18] Gaš, B., Štědrý, M., Kenndler, E., *Electrophoresis* 1997, *18*, 2123–2133.

[19] Burgi, S. D., Chien, R. L., *Anal. Chem.* 1991, *63* 2042–2047.

[20] Taylor, G. I., *Proc. R. Soc. Lond. A* 1953, *219*, 186–203.

[21] Bharadwaj, R., Santiago, J. G., *J. Fluid Mech.* 2005, *543*, 57–92.

[22] Ajdari, A., Bontoux, N., Stone, H. A., *Anal. Chem.* 2006, *78*, 387–392.

[23] Bharadwaj, R., Huber, D. E., Khurana, T., Santiago, J. G., in: Landers, J. P. (Ed.), *Handbook of Capillary and Microchip Electrophoresis and Associated Microtechniques*, CRC Press, Taylor & Francis Group, Boca Raton 2008, pp. 1085–1116.

[24] Yang, H., Chien, R. L., *J. Chromatogr. A* 2001, *924*, 155–163.

[25] Bahga, S. S., Moza, R., Khichar, M., *Proc. R. Soc. A* 2016, *472*, 20150661.

[26] Mani, A., Bazant, M. Z., *Phys. Rev. E* 2011, *84*, 061504.

[27] Saville, D. A., Palusinski, O. A., *AIChE* 1986, *32*, 207–214.

[28] Dubey, K., Gupta, A., Bahga, S. S., *Phys. Fluids* 2017, *29*, 092007.

[29] Sharan, S., Gupta, P., Bahga, S. S., *Phys. Rev. E* 2017, *95*, 023103.

[30] Probstein, R. F., *Physicochemical Hydrodynamics: An Introduction*, John Wiley & Sons, Hoboken, NJ 2005.

[31] Barenblatt, G. I., *Scaling, Self-Similarity, and Intermediate Asymptotics*, Cambridge University Press, Cambridge, UK 1996.

[32] Bercovici, M., Lele, K. S., Santiago, J. G., *J. Chromatogr. A* 2009, *1216*, 1008–1018.

[33] Bahga, S. S., Bercovici, M., Santiago, J. G., *Electrophoresis* 2012, *33*, 3036–3051.

[34] Bercovici, M., Lele, S. K., Santiago, J. G., *J. Chromatogr. A* 2010, *1217*, 588–599.

[35] Milanova, D., Chambers, R. D., Bahga, S. S., Bercovici, M., Santiago, J. G., *Electrophoresis* 2011, *32*, 3286–3294.

[36] He, Y., Lee, H. K., *Anal. Chem.* 1999, *71*, 995–1001.

